Available online at www.sciencedirect.com
SCIENCE DIRECT®
Electrochimica Acta 49 (2004) 3651–3664
ELECTROCHIMICA Acta
www.elsevier.com/locate/electacta

Electrochemical, neutron reflectivity and in situ PM-FT-IRRAS studies of a monolayer of *n*-octadecanol at a Au(1 1 1) electrode surface

I. Zawisza [a], I. Burgess [a], G. Szymanski [a], J. Lipkowski [a,*], J. Majewski [b], S. Satija [c]

[a] *Department of Chemistry and Biochemistry, University of Guelph, Guelph, Ont., Canada N1G2W1*
[b] *MLNSCE, LANSCE-12, Los Alamos National Laboratory, Los Alamos, NM 87545, USA*
[c] *NIST Center for Neutron Research, NIST, Gaithersburg, MD, USA*

Received 6 December 2003; received in revised form 12 February 2004; accepted 22 February 2004

Abstract

The horizontal touch and Langmuir–Blodgett techniques have been used to transfer a monolayer of *n*-octadecanol from the gas–solution interface of a Langmuir trough onto the metal–solution interface of a Au(1 1 1) electrode. Chronocoulometry has been used to determine the charge density at the electrode surface covered by the film of *n*-octadecanol. The surface pressure of this film was calculated from the charge density data and was found to be controlled by the electrode potential. We have demonstrated that by dialing the potential applied to the electrode via a potentiostat the monolayer adsorbed on the surface can be compressed or decompressed. Two states of the monolayer were observed. The transition between these states took place at a film pressure $\sim$12 mN m^{-1}. Neutron reflectometry and polarization modulation Fourier transform infrared reflection absorption spectroscopy have been employed to determine the nature of the two states. The results show that octadecanol molecules form a two-dimensional solid film at all film pressures. At film pressures larger than 12 mN m^{-1}, the film has low compressibility and *n*-octadecanol molecules assume a small tilt angle with respect to the surface normal. At film pressures lower than 12 mN m^{-1} a compressive film is formed in which the tilt angle progressively increases with decreasing surface pressure. We have demonstrated that the properties of a monolayer of *n*-octadecanol at the metal–solution interface display many similarities to the properties of that film at the air–solution interface.

Keywords: Langmuir–Blodgett method; Chronocoulomerty; Photon polarization modulation Fourier transform infrared reflection absorption spectroscopy; Neutron reflectometry

1. Introduction

The past decade has witnessed a significant revival of interest in the properties of monomolecular insoluble films formed by amphiphilic molecules at surfaces [1]. These films are called Langmuir monolayers. They can easily be formed at the surface of a Langmuir trough where their physical state and two-dimensional (2D) ordering can be controlled by mechanical compression. Using either Langmuir–Blodgett or Langmuir–Schaefer techniques [2], the monolayers can be transferred to a solid support to provide well defined coatings for studies of friction, lubrication and wetting, or to build a sensor, protective film and/or a molecular electronics device. Langmuir films can also be deposited onto a metal electrode surface [3–16] and subsequently be exposed to static electric fields on the order of 10^9 V/m. The electric field, or potential applied to the electrode, may be used to force a phase transition in the film, aggregation or desorption of the amphiphiles.

In this paper we apply neutron reflectometry and photon polarization modulation Fourier transform infrared reflection absorption spectroscopy (PM-FT-IRRAS) to investigate field driven transformations in a monolayer of *n*-octadecanol deposited at gold electrode surfaces. Amphiphilic *n*-octadecanol is a representative fatty alcohol, whose structure and phase diagram at the air–water inter-

* Corresponding author. Tel.: +1-519-824-4120 ext. 58543; fax: +1-519-766-1499.
E-mail address: lipkowski@chembio.uoguelph.ca (J. Lipkowski).

0013-4686/$ – see front matter © 2004 Elsevier Ltd. All rights reserved.
doi:10.1016/j.electacta.2004.02.051

face was intensively studied [1,17–24] using compression isotherms in a Langmuir trough [21,25], X-ray diffraction [1,19,20] and Brewster angle microscopy [24]. Langmuir monolayers of *n*-octadecanol show a polymorphism. Depending on the surface pressure and temperature, they may exist in two-dimensional solid, tilted (monoclinic or distorted hexagonal) and non-tilted (hexagonal or orthorhombic) phases [1,21]. The phase transition between tilted and non-tilted states is observed at surface pressures $\sim$12 mN m^{-1} [21]. Below 12 mN m^{-1}, the film forms the so-called L_2 phase in which the molecules are tilted and packed in a distorted hexagonal or a monoclinic sub-cell [1]. Above the phase transition the hydrocarbon chains are aligned perpendicular to the air–water interface [1,21,22]. At temperatures above $\sim$8 °C the vertically oriented molecules are packed in a hexagonal sub-cell (LS); below $\sim$8 °C the packing is orthorhombic (S) [21–24].

For a film of *n*-octadecanol deposited onto a gold electrode surface, we will show that the potential applied to the electrode changes the film pressure. By changing the potential one can compress and decompress the film almost as effectively as by moving a barrier at the surface of a Langmuir trough. By a concerted use of NR and PM-IRRAS techniques we will investigate the potential induced changes in the film structure. We will compare the phase transitions in the monolayer deposited at a gold surface to the phase changes in the film spread at the air–solution interface. We will demonstrate that using a combination of electrochemical, spectroscopic and neutron scattering techniques one can provide a molecular level description of the structure of thin organic films at an electrode surface with unprecedented detail.

2. Experimental

2.1. Reagents and thin film preparation methods

Per-hydrogen *n*-octadecanol (Fluka) was recrystallised form ethanol. It was then dissolved in chloroform (Aldrich) to give $\sim$1.0 mg mL^{-1} stock solutions. A few drops of the stock solution, sufficient to give about three monolayers of *n*-octadecanol, were injected onto the air–solution interface of an electrochemical cell and left for $\sim$30 min to allow the surfactant to spread and the surface pressure to attain the equilibrium spreading pressure, equal to 33 mN m^{-1} [14]. The film was transferred from the air–solution interface to the gold–solution interface using the Langmuir–Schaefer [2,26] (also called the horizontal touch method) as shown in Fig. 1A. To transfer a monolayer at a controlled potential, a dry gold electrode was slowly approached to the film covered air–solution interface until contact with the solution was established. The surface of the electrode was pre-adjusted to be parallel to the surface of the electrolyte and the working electrode potential was preset to 0.0 V (SSCE). After the deposition, the working electrode was elevated (ca. 2 mm) to assume a hanging meniscus configuration and the electrochemical characterization of the surfactant-covered Au(1 1 1) surface was carried out.

In addition, monolayers of *n*-octadecanol were deposited onto the gold electrode surface using the Langmuir–Blodgett technique. A LB trough equipped with a moving barrier and a Wilhelmi plate (KSV, Finland) was employed in these experiments. The trough was controlled by a computer using KSV LB5000 software. The monolayers were prepared at room temperature, 20 $\pm$ 2 °C on the aqueous subphase. The monolayers were compressed to a surface pressure of 35 mN m^{-1} and transferred onto the gold electrode surface by either vertical withdrawing (at speed v = 3 mm min^{-1}) or immersing through the film (at speed v = 8 mm min^{-1}) as schematically shown in Fig. 1B and C, respectively. In all experiments the monolayers of *n*-octadecanol were transferred onto the gold electrode surface with a transfer ratio 1.0 $\pm$ 0.1.

2.2. Electrochemical measurements

The electrochemical measurements were carried out in an all glass three-electrode cell using the hanging meniscus configuration [27]. The Au(1 1 1) crystal served as the working electrode (WE) and a Au wire as the counter electrode (CE). The reference electrode was a silver–silver chloride electrode (SSCE) in the saturated solution of KCl connected to the cell via a salt bridge. The cleanliness of the base electrolyte was checked by cyclic voltammetry and differential capacitance (DC) measurements using the experimental pro-

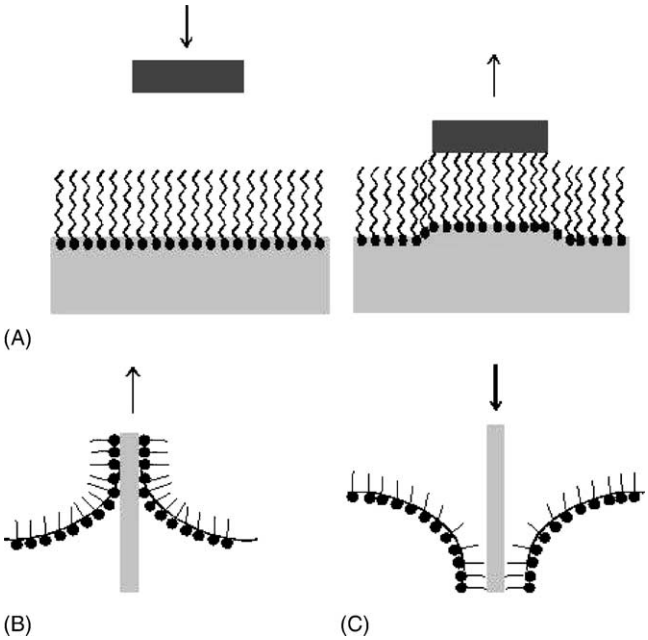

Fig. 1. Scheme of the molecular arrangement in a monolayer on the electrode surface obtained using: (A) the horizontal touch method; (B,C) the Langmuir–Blodgett method by (B) withdrawing, (C) immersing the substrate through the interface covered by the monolayer.

cedures described previously [28]. The cyclic voltammetry curves were recorded at a scan rate of 20 mV s^{-1}. The differential capacity curves were determined using a scan rate of 5 mV s^{-1} and an ac perturbation with 25 Hz frequency and 5 mV r.m.s. amplitude. A computer-controlled system, consisting of a HEKA potentiostat/galvanostat, a HEKA scan generator (Lambrecht/Pfalz, Germany) and a lock-in amplifier, EG&G Instruments 7265 DSP (Cypress, CA), was employed to perform electrochemical experiments. All electrochemical data were acquired via a plug-in acquisition board (National Instruments PCI 6052E) and custom-written software generously provided by Professor Dan Bizzotto of the University of British Columbia. The differential capacity curves were calculated from the in-phase and the out-of-phase components of the ac signal assuming a simple series RC equivalent circuit.

Chronocoulometry was used to determine the charge density at the electrode surface. The gold electrode was held at a base potential $E_b = 0.0$ V for 30 s. Then the potential was stepped to a variable potential of interest E_f, where the electrode was held for a time, t_f, equal to 20 s. Next, a potential step to the desorption potential $E_{des} = -0.725$ V was applied for 150 ms and the current transient corresponding to the desorption of the film and recharging of the interface was recorded. Finally, the potential was stepped back to E_b for 30 s before new potential steps to E_f and from E_f to E_{des} were applied. The integration of the current transients gives the difference between charge densities at potentials E_f and E_{des}. Similar experiments were performed at the film free electrode in the pure supporting electrolyte. The absolute charge densities were then calculated using the independently determined potential of zero charge (pzc) $E_{pzc} = 0.31$ V versus SSCE. The gold single crystal electrode Au(1 1 1) was grown, cut and polished in our laboratory [28]. Prior to experiments the electrode was cleaned by flame annealing. Electrochemical experiments were carried out in 0.1 M NaF supporting electrolyte. IR measurements were performed in 0.1 M NaF dissolved in D_2O (Cambridge Isotopes Ltd.).

2.3. Spectra collection and processing

The details of the PM-IRRAS experiments were described in our previous publication [16]. For clarity we provide here the most important information. The Nicolet, Nexus 870 (Madison, WI) spectrometer, equipped with an external TOM table, MCT-A detector, photoelastic modulator (Hinds Instruments PM-90 with II/ZS50 ZnSe 50 kHz optical head, Hillsboro, OR) and demodulator (GWC Instruments Synchronous Sampling Demodulator, Madison, WI) was used to perform PM-FT-IRRAS experiments. The spectra were acquired using in-house software [29a], an Omnic macro and digital-to-analog converter (Omega, Stamford, CT) to control the potentiostat (HEKA PG285, Lambrecht/Pfalz, Germany) and to collect spectra. The IR window was ~2.5 cm equilateral prism BaF_2 (Janos Technology, Townshead, VT). Prior to the experiment, the window was washed in water and methanol and then cleaned for 20 min in an ozone chamber (UVO-cleaner, Jelight, Irvine, CA). Prior to the assembly of the spectroelectrochemical cell, a monolayer of *n*-octadecanol was transferred onto Au(1 1 1) surface by the horizontal touch method. After the organic film was deposited onto the electrode surface, the cell was filled with the electrolyte and argon was purged through the solution to remove oxygen. The electrode was then pressed against the BaF_2 window to form a thin layer configuration. A starting potential of $E = 0.20$ V(SSCE) was applied to the electrode and spectra were collected in a series of potential steps. Initially, the potential was stepped in the negative direction using a step increment of 0.050 or 0.2 V until a negative potential limit (at which point the film is detached from the electrode surface) was reached. At this point the direction of potential steps was reversed and spectra were collected at 0.050 or 0.2 V intervals up to $E = 0.20$ V (SSCE). For this initial cycle of steps, 1000 scans were recorded at every potential. Subsequently, the cyclic series of potential steps was repeated 20 times so that a total of 8000 scans were recorded at each potential. The instrument resolution was 2 cm^{-1}. At the end of the measurement, before averaging, the scans were individually checked for anomalies using an automated software macro.

Measurements of IR spectra were carried out with the PEM set for half-wave retardation at 2900 cm^{-1} for the CH stretching region and to 1450 cm^{-1} for CH bending modes. At the PEM setting of 2900 cm^{-1}, the 2400–3200 cm^{-1} band-pass filter was employed. In the CH stretching region, the angle of incidence of the infrared beam was set to 52°. The electrolyte thickness between the electrode and the prism was ca. 2.0 μm, giving the highest enhancement of the intensity of p-polarized light on the electrode surface. In the CH bending mode region the angle of incident light was set to 60° and the gap between the prism and the electrode was 3.4 μm.

The demodulation technique developed in Corn's laboratory [30,31] was used in this work. After demodulation two signals were measured: (i) the averaged intensity $I_A(\omega)$; (ii) the intensity difference $I_D(\omega)$. The two signals have to be corrected for the PEM response functions. A modified version of the method described earlier [32] was employed to calculate the PEM response functions. The details of the calculations and the calculated PEM response functions are described in [16]. Furthermore, the signals $I_A(\omega)$ and $I_D(\omega)$ have to be corrected for the difference between the optical throughputs of the optical set-up for p- and s-polarized light [16,32]. The ratio of the throughputs of the optical set-up for p- and s-polarized light was equal to 1.06 [16].

Finally, when in situ experiments are performed in a thin layer cell that contains an electrolyte, the measured spectrum has a background due to the absorption of the IR beam by the aqueous solution in the thin layer. To correct the spectra for the background, a baseline was built for each spectrum using a spline interpolation technique. The same data points

were used to build the spline for all the spectra. When all these corrections are introduced, the background corrected spectrum plots ΔS, which is proportional to the absorbance A of the adsorbed molecules as shown by Eq. (1):

$$\Delta S = \frac{2(I_s - I_p)}{I_s + I_p} = 2.3A = 2.3\Gamma\varepsilon \quad (1)$$

where ε is the decimal molar absorption coefficient and Γ the surface concentration of the adsorbed species. The term 2.3 appears in Eq. (1) as a consequence of the Beer's law written as: $I_R/I_O = 10^{-(\varepsilon\Gamma+\text{const})} = \exp(-2.3\varepsilon\Gamma - 2.3\text{const})$ with I_R and I_O being the intensities of the reflected and incident beams and term "const" representing attenuation of the beam by other than the monolayer components of the optical path [29b].

2.4. Transmission measurements

Fig. 2 shows the isotropic optical constants of *n*-octadecanol obtained using the procedure described by Allara and Swalen [33] for octadecanol dissolved in deuterated methanol (Aldrich). Two ZnSe disks were used as windows of a thin layer cell that had a thickness of 25 μm. The concentration of *n*-octadecanol in CD_3OD was 0.523% (v/v) and 800 spectra with resolution 4 cm^{-1} were recorded. The attenuation coefficient k was determined from the transmission spectra and the refractive index n was calculated from k using the Kramers–Kroenig transformation. For the CH stretching and bending regions the refractive index at infinite frequency n_∞ was taken to be 1.41 [34].

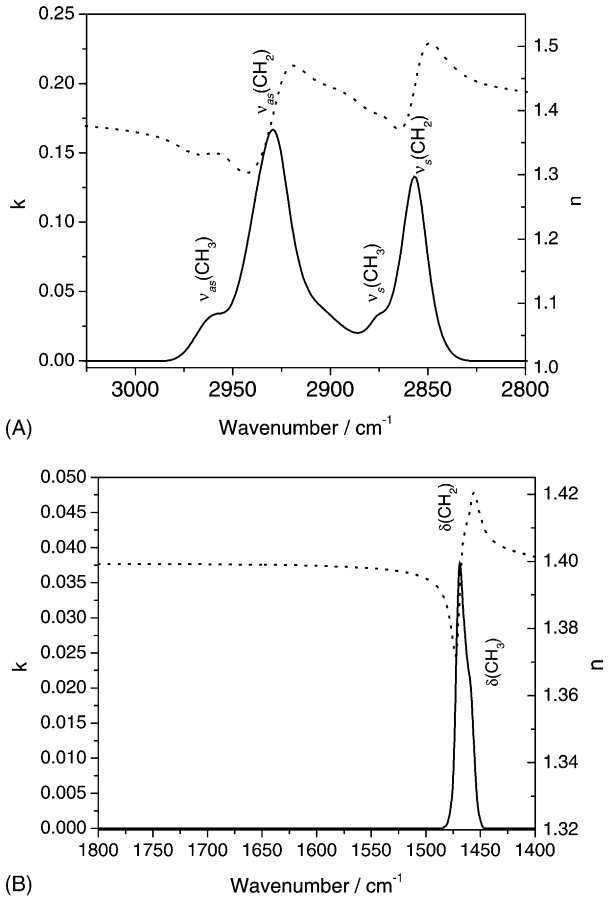

Fig. 2. Isotropic optical constants of *n*-octadecanol calculated from the transmittance of its 0.523 vol.% solution in a CD_3OD (A) CH stretching; (B) CH bending regions; (solid line) attenuation coefficient (k); (dotted line) refractive index (n).

2.5. Neutron reflectivity—methods and experimental

Neutron reflectivity experiments were carried out on the NG-7 reflectometer at the National Institute of Standards and Technology (NIST) in Gaithersburg, Maryland. The working electrode was derived from a polished single crystal (∼ 82 mm × ∼ 38 mm × ∼ 13 mm) quartz substrate obtained from CrysTec GmbH (Berlin, Germany). Thin layers of chromium and gold were sequentially sputtered on the substrates. The resistance of the thin film of gold was on the order of a few ohms. Details concerning the cell design and assembly as well as substrate preparation and cleaning have been provided elsewhere [35].

A film of octadecanol was spread at the surface of water in a small Langmuir trough at the equilibrium spreading pressure and transferred onto the dry, gold-coated surface of the quartz crystal using a single touch, Langmuir–Schaefer technique. The electrolyte solution was 50 mM $KClO_4$ prepared in D_2O (99.9%, Sigma). The electrolyte solution was degassed with argon and then introduced into the inlet of the Teflon cell. The reference electrode was then placed in an arm leading into the Teflon block.

Neutron reflectivity measures the normalized (by the incident flux) intensity of specularly reflected neutrons as a function of the momentum transfer vector Q_z:

$$Q_z = \frac{4\pi \sin\theta}{\lambda} \quad (2)$$

where θ is the angle of the incident and specular reflected neutrons and λ the neutron de Broglie wavelength. A fixed neutron wavelength of 4.75 Å was used. The error points on the data represent the statistical errors in the measurements (standard deviation σ). A constant instrumental resolution of $\Delta Q_z/Q_z = 0.043$ (FWHM) was used throughout the scan. An "inverted" geometry, in which the gold-coated quartz electrode was above the solvent phase, was used in our experiments. Varying the angle of incidence allowed reflectivities to be measured in the Q_z range of ∼0.0 to up to 0.15 $Å^{-1}$. The data was reduced taking into account the neutron beam transmission through the quartz substrate and corrected for the background. The scattering length density (SLD) and the film thickness data were determined by fitting a model to the reflectivity curve using the Parratt 32 fitting algorithm [36]. As a measure of the "goodness of fit" one can calculate the error bar weighted difference between

the experimental (R^{meas}) and calculated curves (R^{cal}) via the following algorithm:

$$\chi^2 = \frac{1}{N}\sum_{i}^{N}\frac{(R_i^{cal} - R_i^{meas})^2}{\delta_i} \quad (3)$$

where δ_i is the error in the measured point and N the total number of experimental points.

3. Results and discussion

3.1. Electrochemistry

We would like to stress that the electrochemical behavior of *n*-octadecanol monolayers transferred from the air–solution interface to the metal–solution interface in $KClO_4$ based electrolytes has been covered in detail by Bizzotto et al. [8–15]. Herein, we include electrochemical results for two reasons: (1) a NaF solution rather than a $KClO_4$ solution had to be used for the PM-FT-IRRAS measurements; (2) the interpretation of the PM-FT-IRRAS and NR results is conveniently explained in terms of the electrochemical characteristics of the transferred *n*-octadecanol monolayers. Fig. 3 shows the electrochemical characteristics of the monolayer film transferred onto the gold–solution interface at $E = 0.0\,V$ (SSCE). The differential capacity curves displayed in panel 3a, indicate that adsorption of *n*-octadecanol at the gold electrode has a two state character. The first state corresponds to $E > -0.1\,V$ (SSCE) where the capacity decreases to a low value of $5.0 \pm 0.5\,\mu F\,cm^{-2}$. The second state is observed between $-0.6\,V < E < -0.1\,V$ (SSCE) and is characterized by a capacity of $\sim 13\,\mu F\,cm^{-2}$. The pseudo-capacitive peak observed at $E \approx -0.1\,V$ (SSCE) corresponds to the transition between the two states. Its position depends somewhat on the direction of the voltage scan and the scan rate. This behavior indicates that the phase transition is relatively slow.

At potentials $E < -0.7\,V$ (SSCE) the capacity of the electrode initially covered by the monolayer approaches the capacity of the surfactant free interface, indicating that the film of octadecanol is desorbed or detached from the electrode surface. When the voltage is scanned in positive direction, the film is re-adsorbed onto the electrode surface. We note small but measurable differences between the differential capacity curves measured in the first scan after the transfer of the monolayer at $E = 0.0\,V$ (SSCE) and in the second and consecutive scans when the monolayer is re-adsorbed after being detached from the gold surface at $E < -0.7\,V$ (SSCE). The minimum value of the capacity in the first scan amounts to $4.8\,\mu F\,cm^{-2}$ while in the second and consecutive scans it increases to $5.3\,\mu F\,cm^{-2}$.

The differential capacity of a perfect monolayer of vertically oriented *n*-octadecanol molecules should be equal to $1.7\,\mu F\,cm^{-2}$ [37]. The measured values of the differential capacity are significantly higher and this behavior

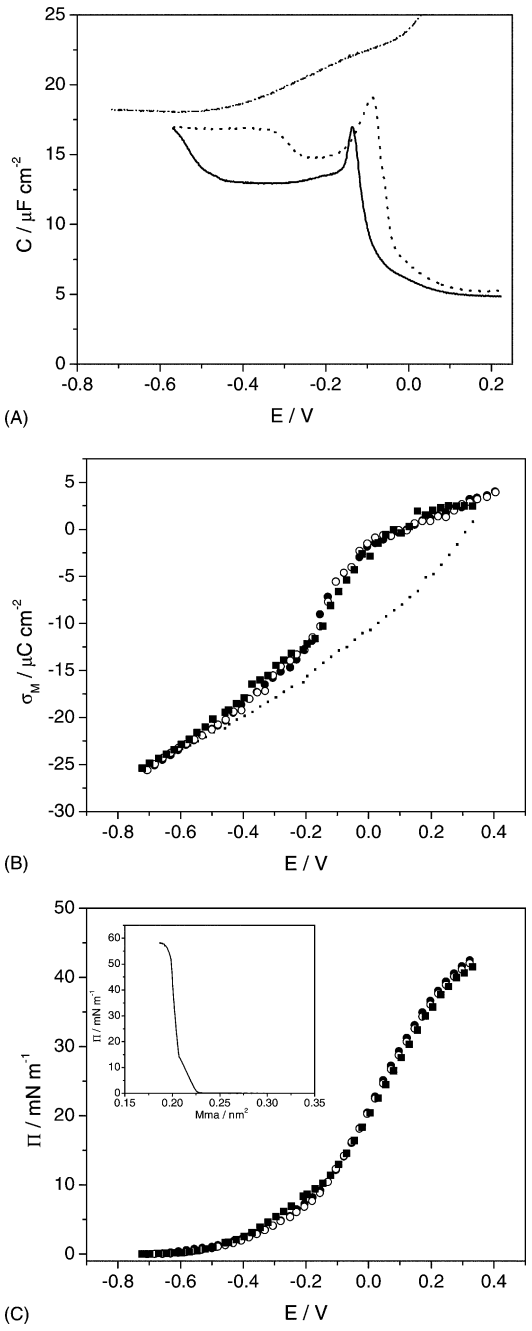

Fig. 3. (A) Differential capacity–potential curves of the monolayer of *n*-octadecanol transferred onto a Au(1 1 1) electrode in 0.1 M NaF/H_2O solution: $v = 5\,mV\,s^{-1}$; $f = 25\,Hz$; $V_{ac} = 5\,mV$ (r.m.s.); negative potential scan (solid line); positive potential scan (dotted line); curve recorded in the absence of the monolayer (dashed line). (B) Charge density and (C) surface pressure–potential plots for an *n*-octadecanol monolayer in the first negative potential steps (filled squares), successive negative (filled circles) and positive (open circles) potential steps, charge density at the film free Au(1 1 1) electrode surface (small squares). Inset of panel C shows the Langmuir isotherm for an *n*-octadecanol film at the air–water interface.

suggests that the film is not perfectly transferred from the gas–solution to the metal–solution interface. The transfer ratio (surface coverage) θ can be estimated with the help of the measured values of the differential capacity using the

formula [38]:

$$\theta = \frac{C_0 - C}{C_{\text{base}} - C_{\text{perfect}}} \quad (4)$$

where C_0 is the capacity in the absence of the surfactant and $C_{\text{perfect}} = 1.7\,\mu\text{F cm}^{-2}$. At $E = 0.2$ V the differential capacity of the gold/0.1 M NaF electrolyte is $32\,\mu\text{F cm}^{-2}$. At this potential the capacity of the monolayer transferred by the horizontal touch method is equal to $4.8\,\mu\text{F cm}^{-2}$ corresponding to the transfer ratio (surface coverage) $\theta = 0.9$.

Panel 3b shows charge density curves determined from chronocoulometric experiments. Three series of measurements were performed. In the first series (full squares) the monolayer was transferred to the gold electrode at $E = 0.0$ V (SSCE) and then the potential was changed to the value E_f plotted in the figure. The charge was measured by stepping the potential from E_f to -0.725 V (SSCE). The electrode was then removed, flame annealed and brought again in contact with the monolayer covered gas–solution interface at $E = 0.0$ V (SSCE). A new (more negative) value of E_f was then applied and the charge corresponding to the potential step to -0.725 V (SSCE) was measured again. For each potential E_f, the charges plotted in panel 3b are the average of three independent measurements. In this series, each charge density point corresponds to the film that was freshly formed at $E = 0.0$ V (SSCE) and desorbed at -0.725 V (SSCE) only once.

In series two and three, the film was formed at $E = 0.0$ V (SSCE) and then a train of potential pulses with a variable amplitude E_f was applied to determine the charge densities. Open circles correspond to the train of pulses with amplitude progressively increasing in the positive direction. Full circles plot charge densities measured when the amplitude of E_f was progressively decreasing moving from 0.4 V (SSCE) in the negative direction. In these experiments, the film was desorbed at -0.725 V (SSCE) and re-adsorbed at E_f many times. Clearly, similar charge density curves were determined in each series of experiments. The charge density curves display two overlapping steps, the small one at $0.5 < E < -0.15$ V (SSCE) and the large one at $-0.15 < E < 0.4$ V (SSCE), that can be assigned to the two states of the film identified earlier with the help of the differential capacity curves. More positive potentials were not applied to avoid oxidation of *n*-octadecanol.

The area between the charge density curves for the supporting electrolyte and the octadecanol film corresponds to the surface pressure of the film, which can be calculated using the formula [28]:

$$\Pi = \gamma_0 - \gamma = \int_{E-0.725}^{E} \sigma_M \, dE - \int_{E-0.725}^{E} \sigma_{M0} \, dE \quad (5)$$

where γ_0 and γ are the surface energies and σ_{M0} and σ_M are the charge densities in the absence and in the presence of the film, respectively. The surface pressure curves are plotted in panel 3c. They are seen to be composed of two overlapping parabolas. A fragment of a small parabola can be seen at negative potentials and film pressures less than $\sim 12\,\text{mN m}^{-1}$ (at $E = -0.12$ V an inflection is observed) and a section of the large parabola with the maximum at ~ 0.2 V can be seen at film pressures larger than $12\,\text{mN m}^{-1}$.

The inset to panel 3c shows the compression isotherm for the monolayer of *n*-octadecanol at the air–solution interface. The film of *n*-octadecanol also forms two states at this interface. The solid tilted film at pressures lower than $12.5\,\text{mN m}^{-1}$ and the solid non-tilted film at higher film pressures [1,21]. Interestingly, the phase transition at the gold–solution and the air–solution interfaces takes place at similar values of the film pressure. This behavior suggests that by changing the electrode potential one can compress or decompress the film at the gold–solution interface in a manner similar to the way the displacement of a movable barrier in a Langmuir trough affects the compression of the film at the air–solution interface. We note that the highest value of the surface pressure of the film at the gold electrode surface amounts to $42\,\text{mN m}^{-1}$ and it is higher than the value of the equilibrium spreading pressure of the film at the air–solution interface ($33\,\text{mN m}^{-1}$). To investigate the origin of this effect, monolayers of *n*-octadecanol were transferred onto the gold electrode surface using the Langmuir–Blodgett technique.

Fig. 4 compares the electrochemical properties of the monolayer transferred using the horizontal touch method (curve 1) with the properties of monolayers transferred by withdrawing the electrode through the film compressed to $35\,\text{mN m}^{-1}$ (curve 2) and by immersing the electrode through the film (curve 3). Although the three films display qualitatively similar electrochemical behavior, one notes that the lowest capacity, the largest change in the charge density and the highest film pressures are observed for the film transferred by the horizontal touch method. The lowest value of the surface pressure is observed for the LB film transferred by withdrawing the electrode through the film ($30\,\text{mN m}^{-1}$) when the OH groups are directed to the metal. Intermediate values of surface pressures are observed for the film transferred by immersing the electrode through the monolayer at the trough surface and withdrawing it through the decompressed surface (molecules oriented with the hydrocarbon tails turned toward the metal). However, for this film, the electrode capacity and the charge density curves show a steep rise at $E > 0.1$ V. This behavior suggests that the film may be oxidized at these positive potentials.

This hypothesis is confirmed by recording the IR spectrum of the monolayer of *n*-octadecanol recorded at $E = 0.2$ V, as presented in Fig. 5. The spectrum shows bands of the carbonyl stretch and the asymmetric and symmetric stretches of the carboxylic group that were absent in the transmission spectrum of pure octadecanol (see Fig. 2b). Their presence indicates that a partial oxidation of this surfactant takes place at the gold electrode surface at higher positive potentials.

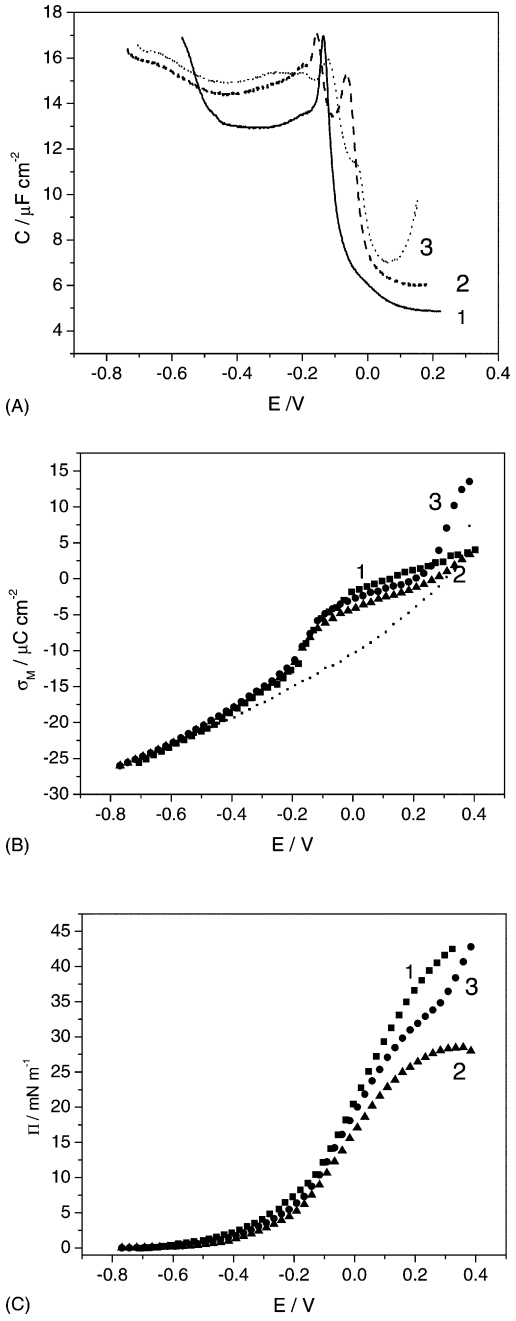

Fig. 4. (A) Differential capacity; (B) charge density; (C) surface pressure vs. potential plots of a monolayer of *n*-octadecanol transferred onto the Au(1 1 1) electrode using: (1) the horizontal touch method; (2,3) the Langmuir–Blodgett method—(2) withdrawing; (3) immersing of the gold. The electrolyte solution was 0.1 M NaF in H_2O.

To summarize this section, electrochemical measurements demonstrate that a monolayer of *n*-octadecanol transferred from the gas–solution interface is defected. This is not an unexpected result because recent Brewster angle microscopy studies of *n*-octadecanol monolayers at the air–solution interface demonstrated that the film also has many defects at the air–solution interface [39]. However, at the gold–solution interface, at positive potentials, the film may be partially

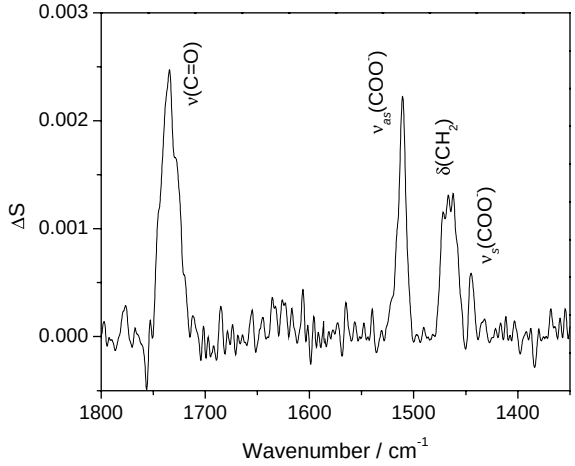

Fig. 5. The PM-FT-IRRAS spectrum in the carbonyl stretching and CH bending region of a monolayer of *n*-octadecanol on the Au(1 1 1) surface at $E = 0.2$ V (SSCE) in 0.1 M NaF/D_2O.

oxidized and then it may have an admixture of aldehydes and carboxylic acids. The shift of the pzc in the negative direction and consequently somewhat higher values of the surface pressure for the horizontal touch film may be explained by the presence of ionized carboxylic groups in the film (the pH of the solution is ∼9). At this pH, at the film free Au(1 1 1) surface the onset of OH^- adsorption is observed at $E \sim -0.2$ V. Initially, the coverage of OH is small and changes slowly with potential and then increases steeply at $E > 0.2$ V [40]. In the presence of a monolayer the OH adsorption should be blocked, however at defects a partial oxidation of the *n*-octadecanol molecules may already take place at quite low potentials.

3.2. Neutron reflectivity—results and discussion

Neutron reflectivity (NR) experiments were performed in an effort to determine the thickness of the octadecanol film formed by the horizontal touching technique. A detailed explanation of our treatment of neutron reflectivity data has been given recently [35]. Briefly, the specular reflection of monochromatic neutrons provides information on the nuclear composition of the interface in the direction perpendicular to the surface (denoted as the *z*-direction). Using the kinematic approach [41,42] it can be shown that the precise relationship between the intensity of reflected neutrons (R) to the nuclear composition is given by Eq. (6):

$$R(Q_z) = \frac{(4\pi)^2}{Q_z^4} f(\rho) \tag{6}$$

in which the first term (proportional to ${Q_z}^{-4}$) describes the Fresnel reflectivity from a single interface and the second term is a function of the SLD (ρ) profile in the direction normal to the surface. The SLD is determined by the combined nuclear spin state of the nucleus–neutron scattering system

and consequently depends on the nuclear composition of the film.

The function $f(\rho)$ in Eq. (6) is not readily evaluated. The commonly used approach to analyze NR data is to build a model of the interface consisting of discrete layers and calculate the reflectivity using an analogous approach to the optical matrix method [43] or using Parratt's recursion method [44]. The model is compared to the measured reflectivity and the layer parameters (film thickness and SLD) are adjusted to give a best-fit using non-linear, least squares regression.

In our treatment of the neutron reflectivity of octadecanol monolayer films we fixed the thickness of the Cr and Au layers as these were determined independently by X-reflectivity measurements. The roughness of the quartz substrate was determined by X-ray reflectivity to be 5 Å. This root mean square roughness was then fixed as an overall roughness for the chromium and gold modified electrode. Because the SLDs of both quartz and D_2O are known, the only adjustable parameters in the fitting were the thickness of the octadecanol film and the SLDs of the Cr, Au and organic layers.

Fig. 6A presents the results of the NR experiment performed on an octadecanol monolayer formed by the horizontal touch procedure when the electrode potential was held at +100 mV (versus SSCE). The points with associated error bars represent the experimentally obtained data whereas the solid line is the reflectivity calculated from the best-fit model of the interface. To eliminate the fast Fresnelian decay of the reflectivity it is convenient to multiply the reflectivity by Q_z^4. The inset in Fig. 6A shows the same data as in the main figure but now the fast decay of the reflectivity with the momentum transfer vector has been removed. In either representation it is seen that the best-fit curve and the experimentally measured curve are in very good agreement. The best-fit parameters for $E = +100$ mV (SSCE) are shown in Table 1 and graphically represented in Fig. 7 as an SLD profile (SLD versus z position). The best-fit results indicate that the gold and chromium layers have SLDs close to the theoretical values (4.51×10^{-6} and 3.01×10^{-6} Å^{-2}, respectively). More importantly, the thickness of the organic layer is found to be 22.3 Å which corresponds to a tilt angle of 8° and indicates that the octadecanol layer transferred to the electrode via the horizontal touch method is vertically oriented. Additionally, the volume fraction, x, of D_2O can be estimated by assuming that the organic layer is a binary component system of D_2O and octadecanol.

$$\rho_{\text{total}} = x\rho_{\text{solvent}} + (1 - x)\rho_{\text{org}} \quad (7)$$

The SLD for a compact (20 Å^2/tail) layer of hydrocarbons (ρ_{org}) is equal to -0.49×10^{-6} Å^{-2}. For the NR measurement at $E = +100$ mV we see that the volume fraction of D_2O is 47%.

Fig. 6B shows the experimental and the best-fit curves for the same octadecanol film but now at a potential $E = -300$ mV. Comparison of Fig. 6A and B indicates that there is a systematic decrease in the overall reflectivity of the curve measured at the more negative potential. This is explained by a decreased contrast in the scattering length densities

Table 1
Thickness and scattering length density values for chromium, gold and the organic layer

System	Chromium		Gold		Organic film			χ^2
	τ[a]	SLD[b]	τ[a]	SLD[b]	τ[a]	SLD[b]	x	
$C_{18}OH$, $E = 100$ mV	35	3.65	75	4.56	22.3	2.69	0.47[c]	4.7
$C_{18}OH$, $E = -300$ mV	35	3.65	75	4.56	21.4	3.61	0.60[c]	1.9

[a] Thickness of layer in Å.
[b] Scattering length density $\times 10^6$ Å^{-2}.
[c] Volume fraction of solvent.

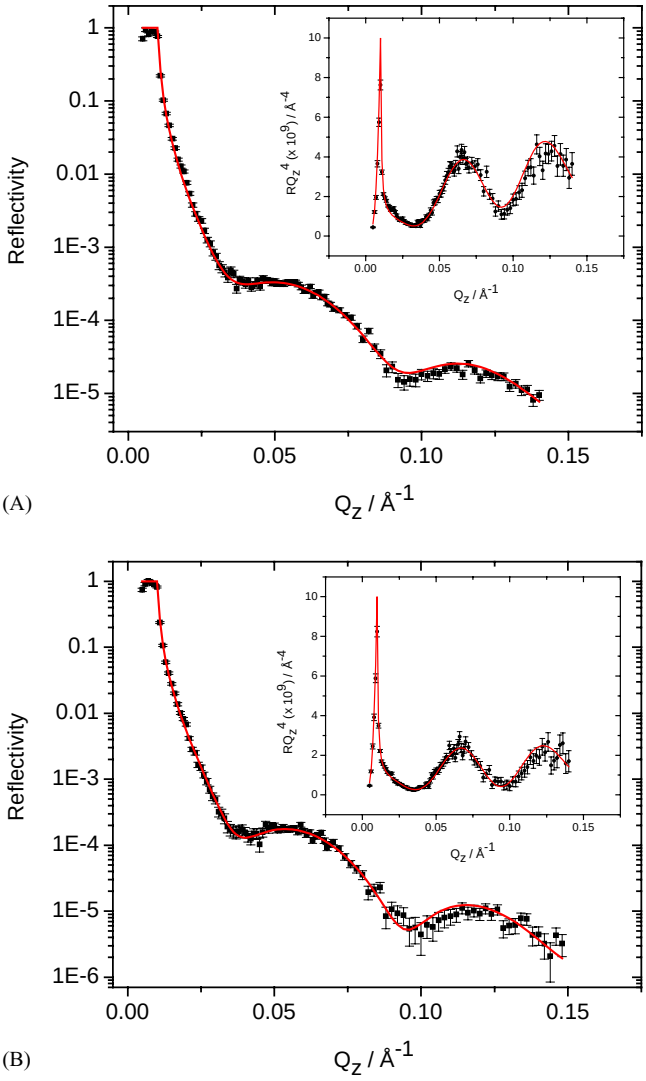

Fig. 6. Neutron reflectivity curves obtained for a monolayer of per-hydrogen *n*-octadecanol deposited onto a gold-coated block of quartz. The electrolyte solution was 0.05 M $KClO_4$ in D_2O; Panel A at $E = 0.1$ V and panel B at $E = -0.3$ V. Insets display the same reflectivity data plotted as RQ^4 in order to eliminate the fast Fresnelian decay of the reflectivity. Points with associated error bars are the experimental data, solid lines show the best-fit curves.

of the organic film and the electrolyte backing. Indeed, the best-fit analysis reveals that the SLD of the octadecanol film at $E = -300$ mV has risen by nearly 40%. This observation is consistent with an increased solvent occupancy in the film and by employing Eq. (7) we see that the volume fraction of D_2O has risen to 60%. It is interesting to note that the film thickness has decreased to 21.4 Å corresponding to an 18° tilt angle. The neutron reflectivity experiments indicate that the octadecanol monolayer becomes more defected (i.e. an increased level of solvent) and more tilted (18° versus 8°) when the potential is dialed to −300 mV versus SSCE. These potential dependent changes are shown in the SLD profiles shown in Fig. 7.

The neutron reflectivity data reveals that the monolayer of *n*-octadecanol, transferred onto the gold-coated block of quartz is patchy. Recently we described similar problems with the formation of a patchy monolayer of 4-pentadecyl-pyridine at the gold-coated block of quartz [35]. The reflectivity data for a patchy adsorbed layer at the interface can still be modeled and analyzed in terms of stratified media as long as the area of the patches is smaller than the transverse coherence length of the neutrons. The neutron coherence length is the distance over which the neutron wavefront can considered planar and for the range of Q_z values employed, it lies between 10 and 100 μm. The agreement between the tilt angles determined from the neutron reflectivity data and the PM-IRRAS experiments described below indicates that in our experiments the size of the defects were less than the coherence length.

3.3. IR spectroscopy

3.3.1. CH stretching spectra of the n-octadecanol monolayer

Fig. 8 plots the PM-FT-IRRA spectra in the CH stretching region of *n*-octadecanol monolayer. Fig. 8A shows spectra acquired for a freshly deposited film by changing the potential from 0.2 V (SSCE) in the negative direction (desorption scan). Fig. 8B shows spectra recorded when the potential is again changed from 0.2 V (SSCE) in the negative direction (re-desorption scan) following re-adsorption of the previously desorbed film. For comparison, the thick solid line in Fig. 8A plots the reflection absorption spectrum of randomly oriented *n*-octadecanol molecules calculated from the optical constants presented in Fig. 2, assuming that the thickness of the film is equal to 2.49 nm [45] and using the angle of incidence and the thickness of electrolyte layer determined at the beginning of the PM-FT-IRRAS experiment.

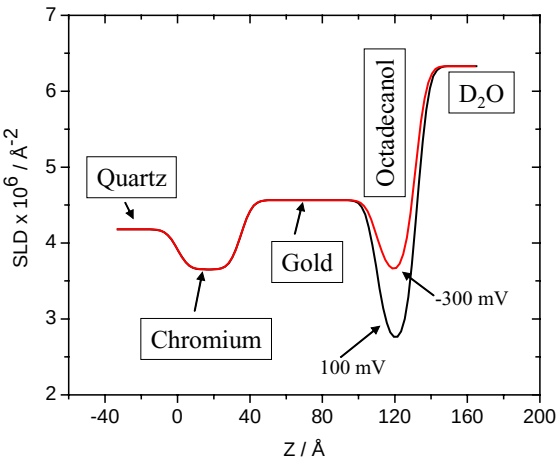

Fig. 7. The SLD profiles determined from the best-fit of a model to the reflectivity data.

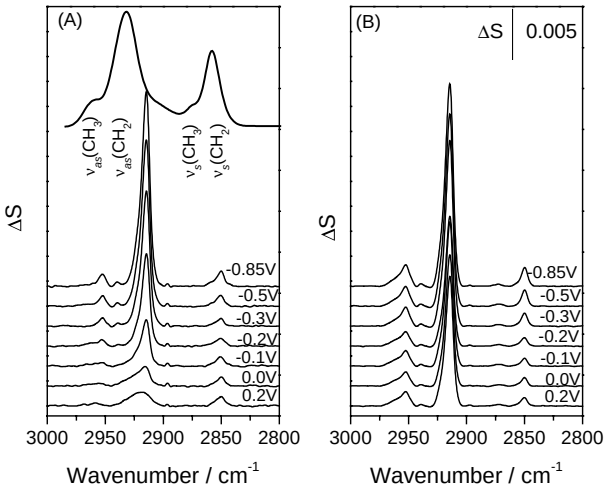

Fig. 8. PM-FT-IRRAS spectra in the CH stretching region for the monolayer of *n*-octadecanol on Au(1 1 1) surface at different potentials marked in the figure: (A) first; (B) successive negative potential steps; (thick line) spectrum calculated from the optical constants for the randomly distributed molecules in the monolayer thick film (2.5 nm) at the Au electrode surface in the stratified BaF_2/D_2O/Au three-phase system, thickness of the D_2O layer 2.2 μm and the angle of incidence 53°, convergent beam with a 5° convergence angle.

In the transmission spectrum of the solution of *n*-octadecanol, the positions of CH stretching bands are: $\nu_{as}(CH_3)$ at 2959.9 cm^{-1}; $\nu_{as}(CH_2)$ at 2932.9 cm^{-1}; $\nu_s(CH_3)$ at 2876.0 cm^{-1} and $\nu_s(CH_2)$ at 2857.9 cm^{-1}. In the monolayer deposited at the gold electrode surface, the frequencies of the CH stretch bands corresponding to $\nu_{as}(CH_3)$, $\nu_{as}(CH_2)$, $\nu_s(CH_3)$ and $\nu_s(CH_2)$ are centered around 2958 cm^{-1}, ~2915 cm^{-1}, 2872 cm^{-1} and 2850 cm^{-1}, respectively. The $\nu_{as}(CH_2)$ peak is asymmetric with the shoulder appearing around 2930 cm^{-1} originating from the Fermi resonance between the symmetric methyl stretch fundamental frequency and the overtones of the methyl asymmetric bending modes [46,47]. In the spectra for the monolayer transferred to the gold surface from the gas–solution interface, similar band frequencies are observed for the freshly formed and re-adsorbed film. Although, the band positions are independent of potential, they are significantly red shifted with respect to the frequencies of the corresponding bands in the spectrum calculated from the optical constants. The position of the CH_2 stretching bands is sensitive to conformational changes of alkyl chains [46,48]. The frequencies of $\nu_{as}(CH_2)$ less than 2920 cm^{-1} and $\nu_s(CH_2)$ less than

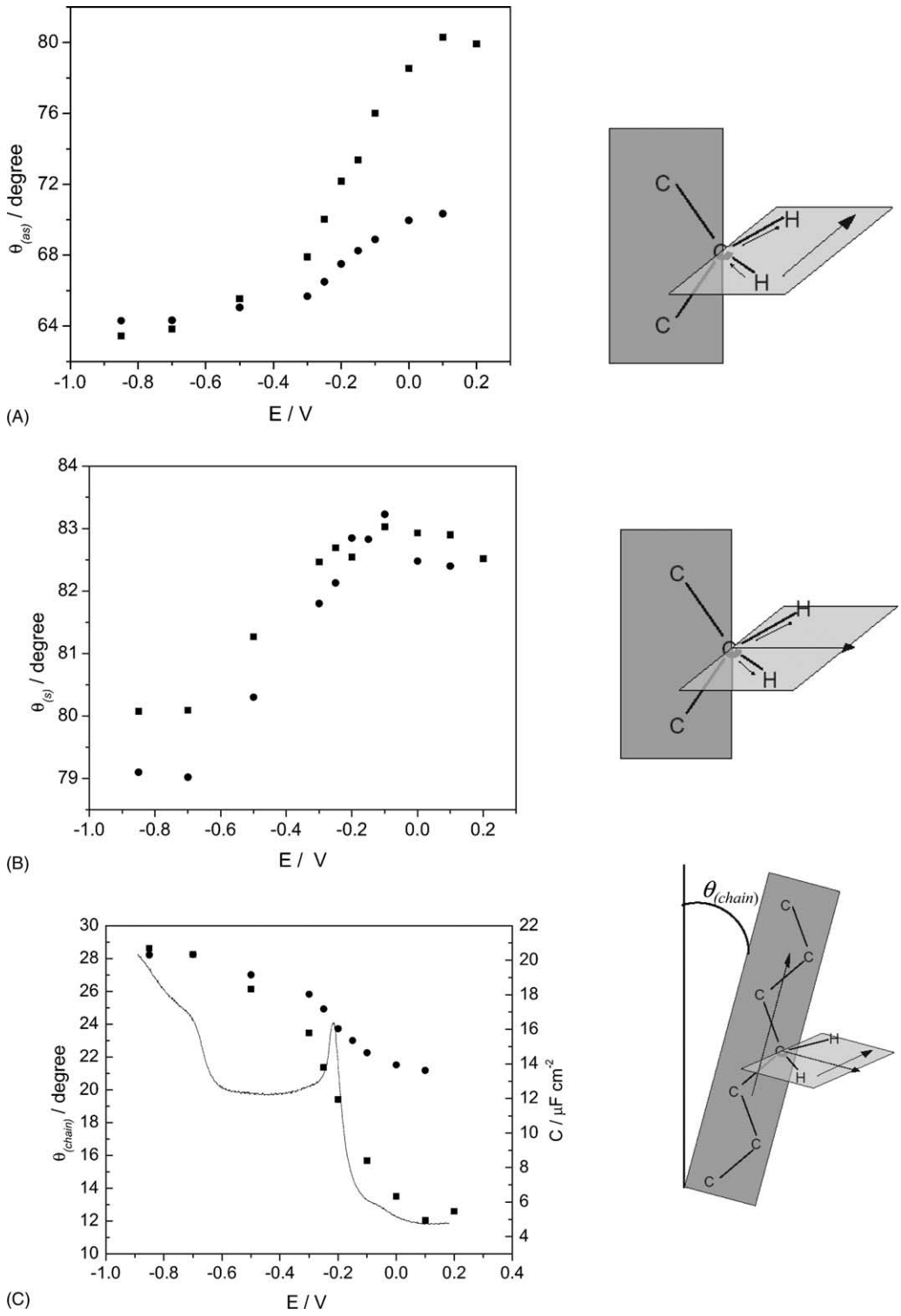

Fig. 9. For a monolayer of *n*-octadecanol at the Au(1 1 1) surface, the angle (θ) between the direction of the transition dipole moment and the electric field of the photon (surface normal) plotted vs. the electrode potential: (A) $\nu_{as}(CH_2)$; (B) $\nu_s(CH_2)$. (C) Changes of the tilt angle of the hydrocarbon chains (filled circles and filled squares) and the differential capacity curve (solid line) vs. potential. In panels (A–C) the points corresponding to the first negative potential steps are represented by (filled squares) and the points corresponding to the first positive potential steps are represented by (filled circles). Illustrations for the pertinent transition dipole moment are shown for each vibration.

2851 cm^{-1} indicate that monolayers of *n*-octandecanol are in the two-dimensional solid state and that the hydrocarbon chains are fully stretched in an all trans zigzag orientation [46].

The CH_2 stretching bands in the spectra of the monolayer of *n*-octadecanol are significantly narrower than the corresponding bands in the spectrum of the solution species. In the transmission spectrum of dissolved *n*-octadeconal (spectrum calculated from the optical constants), the full-width at half maximum (FWHM) is equal to 19.0 cm^{-1} for the asymmetric and equal to 14.2 cm^{-1} for the symmetric methylene stretches. In the film spread on the Au(1 1 1) surface, the FWHM of the $\nu_{as}(CH_2)$ is equal to 7.2 ± 0.2 cm^{-1} and of the $\nu_s(CH_2)$ to 5.7 ± 0.2 cm^{-1}. The half width of the IR bands is determined chiefly by collision broadening. It results from the perturbation of energy levels of the absorbing molecules by a collision with another molecule or a fragment of the same molecule [49]. Therefore, the band narrowing indicates restricted mobility of the alcohol molecules in the monolayer adsorbed on the electrode surface, consistent with the solid state nature of this film.

The relative intensity of the $\nu_{as}(CH_2)$ and $\nu_s(CH_2)$ bands in the spectra for monolayers transferred to the gold electrode and in the spectrum calculated for randomly oriented molecules is distinctly different. The ratio of the integrated band intensities for randomly oriented molecules in solution is equal to 2.7. For the freshly deposited film at $E = 0.2$ V this ratio increases to ~4 and in the re-adsorbed film to 20. This behavior indicates that the *n*-octadecanol molecules in the monolayer deposited on the gold electrode surface are rotationally frozen [50]. For the freshly formed film, the intensity of the $\nu_{as}(CH_2)$ band changes significantly with potential. The changes with potential are much smaller in the re-adsorbed film. The intensities of the $\nu_s(CH_2)$ band also display much smaller dependence on the electrode potential. This behavior points to pronounced changes in the orientation and/or rotation of *n*-octadecanol molecules in the freshly formed and the re-adsorbed films.

The angle between the direction of the transition dipole moment and the direction of the electric field vectors (θ) can be calculated from the integrated intensities of the IR bands using the following equation [33,51]:

$$\cos\theta = \frac{1}{3}\frac{A_{(E)}}{A_{(\text{random})}} \tag{8}$$

where: $A_{(E)}$ equals the integrated intensity of the IR band at a given potential, $A_{(\text{random})}$ equals the integrated intensity of the peak for a random distribution of molecules in the film. The directions of transition dipole moments of the asymmetric and the symmetric CH_2 stretches are orthogonal to each other and form a 90° angle with the line of a fully extended all trans hydrocarbon chain. Therefore, the angles θ_{as} and θ_s and the tilt angle of the chain θ_{chain} are related by the formula [52]:

$$\cos^2\theta_{as} + \cos^2\theta_s + \cos^2\theta_{chain} = 1 \tag{9}$$

from which the tilt angle of the chain can be calculated. Fig. 9 shows the dependence of θ_{as} (panel A), θ_s (panel B) and θ_{chain} (panel C) on the electrode potential. Full squares mark the first desorption scan (voltage scanned in negative direction) and the full circles mark the first re-adsorption scan (voltage scanned in the positive direction). The diagrams in Fig. 9 show the directions of the two transition dipoles and illustrate how the chain tilt angle is defined. To facilitate the comparison of spectroscopic and electrochemical data, the differential capacity curve recorded during the desorption of the freshly formed film is also plotted in panel 9C.

For a freshly deposited monolayer at $E = 0.0$ V (SSCE), the transition dipoles of both $\nu_{as}(CH_2)$ and $\nu_s(CH_2)$ form a large angle θ (~80° and ~84°) with respect to the surface normal and the hydrocarbon chains stand almost vertically assuming a small tilt angle of ~12°. This number compares well with the tilt of 8° determined from neutron reflectivity experiments. By moving E in the negative direction, the angles θ_{as} and θ_s decrease and the chain tilt angle increases. For the freshly formed film, the changes θ_{as} and θ_{chain} with potential are much more pronounced than for the re-adsorbed film. In contrast, the changes of θ_s are small and are of comparable magnitude for the freshly formed and the re-adsorbed films. The significant difference between the magnitude of θ_{as} and θ_s is a result of the restricted rotation in the *n*-octadecanol molecules. Fig. 9C shows that the changes in the tilt angle correlate very well with changes in the differential capacity. The spectroscopic data clearly show that the phase transition seen in the differential capacity (or charge density) curves involves a significant change in the tilt angle. In a good analogy to the behavior of the film at the air–solution interface, the phase transition may be identified as a transition between the vertical and tilted film. Finally, it is useful to note that at $E = -0.3$ V, the tilt angle is 23°. A somewhat smaller angle of 18° was determined from the neutron reflectivity experiments. However, PM-FT-IRRAS and NR measurements report almost the same change of the tilt angle ~10°–11° between $E = 0.1$ and -0.3 V.

To compare monolayers of *n*-octadecanol at the gold–solution and the metal–solution interfaces, the chain tilt angles are plotted as a function of the surface pressure in Fig. 10. The dependence of the tilt angle on the film pressure at the gold–solution interface is shown in Fig. 10A. The tilt angles at the air–solution interface are taken from the literature. They were measured using X-ray diffraction [22,24] or Brewster angle autocorrelation spectroscopy [24] techniques and their values are plotted versus the surface pressure in Fig. 10B. At the two interfaces, a significant change of the tilt angle takes place at surface pressures equal to 12–13 mN m^{-1}. In addition, in the tilted state (at $\pi < 13$ mN m^{-1}) the changes of the tilt angle with the surface pressure are of comparable magnitude at the air–solution and for the freshly formed film at the gold–solution interface.

There also are differences between properties of the film at the two interfaces. At the air–solution interface, the change

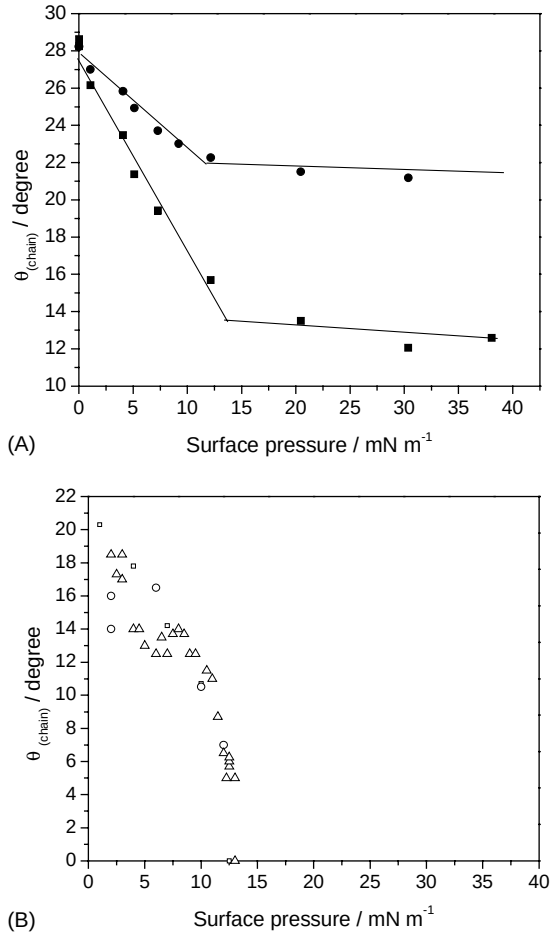

Fig. 10. (A) For the monolayer of *n*-octadecanol at (A) Au(1 1 1) electrode and (B) air–solution interface, dependence of the tilt angle of hydrocarbon chains on the surface pressure: (A) tilt angles determined from PM-FT-IRRAS experiments; the first negative scan (filled squares), successive negative scans (filled circles); (B) literature values of tilt angles determined by: Brewster angle autocorrelation spectroscopy [24] (open triangles), grazing incidence X-ray diffraction [24] (open circles), X-ray diffraction [22] (open squares).

from the vertical (zero tilt angle) to the tilted state is discontinuous. At the metal–solution interface the change from an initial tilt of ∼12° to higher tilt angles is gradual. At the gold–solution interface, the gradual change of the tilt angle may be caused by the presence of impurities, due to the residual oxidation of the *n*-octadecanol film. In addition, defected sections of the film may contribute to the measured initial tilt of ∼12° at $\pi > 13\,\mathrm{mN\,m^{-1}}$. The X-ray diffraction technique, employed to determine the tilt angle in the film at the air–solution interface, probes only ordered domains. In contrast, IR reflection spectroscopy measures the average tilt angle for all molecules at the surface, both in ordered and disordered domains.

The similarity between the tilt angle versus surface pressure plots determined for the gold–solution and the air–solution interfaces indicates that, at the metal–solution interface, the film is compressed or decompressed by a change in the electrode potential (charging of the metal surface) in an analogous fashion to the compression and decompression of the film at the air–solution interface by the movement of the barrier in a Langmuir trough. The decompression (compression) is driven by the energy supplied per unit surface area. In a Langmuir trough, mechanical energy is used to change the state of the film. Our result shows, that at the metal–solution interface, electrical energy may be employed to impose a similar change in the film structure. At the surface of a Langmuir trough the film may be compressed–decompressed reversibly, provided the barrier is moved sufficiently slowly. Similarly, at the metal–solution interface, the film may be desorbed and re-adsorbed reproducibly by applying the electrode potential. However, our data show that the re-adsorbed film contains more defects (larger tilt angle) than the film freshly transferred from the gas–solution interface. Apparently, more ordered films are formed at the air–solution interface when they are compressed by a mechanical force than at the metal–solution interface where the compression is achieved with the help of the electrical energy.

Fig. 11 shows the PM-IRRAS in the region of the asymmetric stretch of the terminal methyl group $\nu_{as}(CH_3)$. For comparison the band in the spectrum calculated for randomly oriented molecules (calculated from the transmission spectrum of the solution of *n*-octadecanol) is also included in this figure. In the spectrum of the solution species, this band overlaps with the $\nu_{as}(CH_2)$ band. To facilitate further discussion, the CH stretching bands in the spectrum for the solution species have been de-convoluted and the de-convoluted $\nu_{as}(CH_3)$ band is plotted in Fig. 11.

In the isolated *n*-octadecanol molecule, the terminal CH_3 group has rotational freedom and C_{3V} symmetry [47]. One symmetric $\nu_{as}(CH_3)$ band with a FWHM equal to $17.2\,\mathrm{cm^{-1}}$ is seen in the spectrum. In the spectrum of the monolayer, the $\nu_{as}(CH_3)$ band is asymmetric and can be de-convoluted into two overlapping bands located at $2952.2 \pm 0.2\,\mathrm{cm^{-1}}$ and $2957.5 \pm 0.2\,\mathrm{cm^{-1}}$. Fig. 11B plots the separation between the two de-convoluted bands as a function of the electrode potential. The change of the FWHM of these bands with potential is shown in Fig. 11C. Clearly, in the spectrum of the monolayer, the $\nu_{as}(CH_3)$ bands are narrower than in the spectrum of the solution species. The separation of these bands increases slightly by moving from the tilted to the non-tilted state.

The narrowing and the split of the asymmetric methyl stretch band were observed in spectra of crystalline *n*-paraffins. They are attributed to restricted rotation of the terminal methyl group [47]. When the mobility of the CH_3 group is restricted, its symmetry is lowered to C_1 and the $\nu_{as}(CH_3)$ band splits into two bands. The $\nu_{as}(CH_3)_a$ band at higher frequencies ($\sim 2960.0\,\mathrm{cm^{-1}}$) has the transition dipole moment parallel to the plane in which the zigzag of the hydrocarbon skeleton is located. The transition dipole of the lower frequency band $\nu_{as}(CH_3)_b$ (at $\sim 2952\,\mathrm{cm^{-1}}$) is directed out of the zigzag plane [47,48,50].

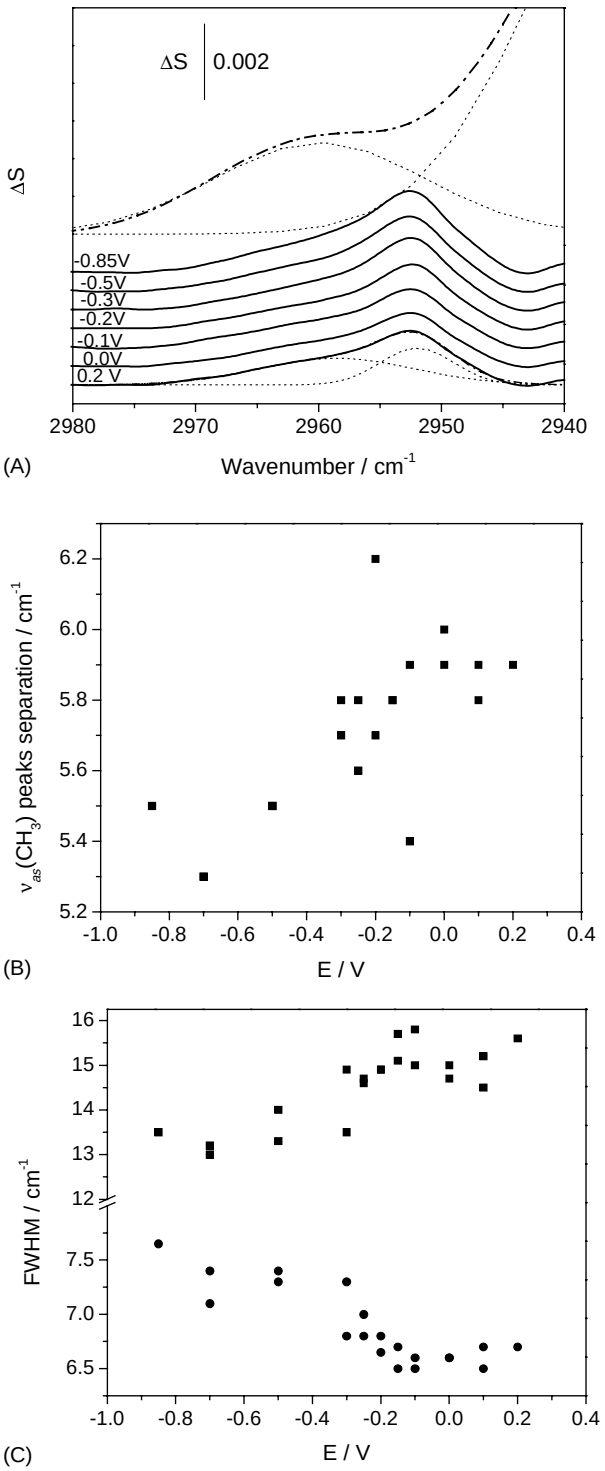

Fig. 11. For the monolayer of *n*-octadecanol at the Au(1 1 1) surface: (A) The $\nu_{as}(CH_3)$ band in the PM-FT-IRRA spectra at several potentials indicated in the figure (solid lines), calculated spectrum for the randomly distributed monolayer (dashed dotted line), deconvoluted spectra (dotted lines); (B) separation between the two de-convoluted $\nu_{as}(CH_3)$ bands plotted against potential; (C) dependence of the FWHM of the deconvoluted $\nu_{as}(CH_3)$ band (peak at 2957 cm^{-1} (squares); at 2952 cm^{-1} (circles) on the electrode potential).

Fig. 11B shows that the peak separation is ∼6 cm^{-1}. Such splitting is expected when rotation of the methyl group is restricted by an interaction with the chain. The width of the $\nu_{as}(CH_3)_b$ band (∼7 cm^{-1}) is also comparable to the width of the motionally narrowed methyl bands in *n*-alkanes [47]. The data in Fig. 11B and C show that the separation increases and the width of the $\nu_{as}(CH_3)_b$ band decreases when $E > -0.3$ V and the transition from the tilted to the non-tilted state takes place. Such behavior suggests that the rotational mobility of the methyl group is more restricted in the non-tilted state of the film. However, the width of the $\nu_{as}(CH_3)_a$ band centered at 2960.0 cm^{-1} is comparable to the width of the $\nu_{as}(CH_3)$ band in the solution species. That band is not significantly narrowed. This behavior suggests that a fraction of *n*-octadecanol molecules in the film contain methyl groups whose rotation is restricted and a fraction of molecules whose methyl groups can rotate. The $\nu_{as}(CH_3)_a$ band and the band of the rotationally unrestricted methyl group have similar frequencies and in the mixed film the two bands can not be separated.

4. Summary and conclusions

We have demonstrated that a monolayer of *n*-octadecanol spread at the air–solution interface can be transferred onto the surface of a Au(1 1 1) electrode using either a horizontal touch or a Langmuir–Blodgett technique with a transfer ratio ∼1. Lower transfer ratios were observed when the film was transferred onto a large surface area gold-coated block of quartz. Electrochemical measurements allow one to determine the surface pressure of the film at the gold surface. The properties of the film at the electrode surface may be then correlated with the surface pressure. Our results show that the monolayer of *n*-octadecanol displays a two-state behavior. The transition between the two states is observed at ∼12 mN m^{-1}. Neutron reflectivity and PM-FT-IRRAS experiments were performed to identify the nature of the two states. These data revealed that at film pressures higher than 12 mN m^{-1} the octadecanol molecules assume a nearly vertical orientation in which the chains form a small tilt angle ∼10° with respect to the surface normal. Here, the tilt angle is essentially independent of the surface pressure. In contrast, at $\Pi < 12$ mN m^{-1} a tilted state is observed in which the tilt angle increases progressively with decreasing film pressure.

We have demonstrated that a monolayer of *n*-octadecanol displays similar properties at the metal–solution and at the air–solution interfaces. The potential applied to the electrode surface changes the surface pressure in a manner analogous to the action of a movable barrier in a Langmuir trough. In the first case, the surface pressure is changed due to the supply/withdrawal of electrical energy and in the second case it responds to the action of a mechanical force. However, more ordered films are formed at the air–solution interface as a result of the mechanical compression than at

the metal–solution interface as a result of the electrochemical compression. We have demonstrated that a combination of electrochemical, neutron reflectivity and PM-IRRAS experiments allows one to understand the nature of the potential induced changes in the structure of a monolayer of amphiphilic molecules at a molecular level.

Acknowledgements

We would like to thank Professor Dan Bizzotto (University of British Columbia) for supplying us with the software used to collect the electrochemical data. This work was supported by a grant from Natural Sciences and Engineering Research Council of Canada. J.L. acknowledges CFI for a Canada Research Chair Award.

References

[1] V.M. Kaganer, H. Mohwald, P. Dutta, Rev. Modern Phys. 71 (1999) 779.
[2] G. Roberst (Ed.), Langmuir–Blodgett Films, Plenum Press, New York, 1990.
[3] R. Parsons, I.R. Miller, J. Coll. Interf. Sci. 45 (1973) 126.
[4] X. Zhang, A. Bard, J. Am. Chem. Soc. 111 (1989) 8098.
[5] C.A. Widrig, C.J. Miller, M. Majda, J. Am. Chem. Soc. 110 (1988) 2009.
[6] D.H. Charych, E.M. Landau, M. Majda, J. Am. Chem. Soc. 113 (1991) 3340.
[7] R. Bilewicz, M. Majda, J. Am. Chem. Soc. 113 (1991) 5464.
[8] D.H. Charych, C.A. Goss, M. Majda, J. Electroanal. Chem. 323 (1992) 339.
[9] K. Slowinski, R. Bilewicz, M. Majda, Chem. Anal. 40 (1995) 329.
[10] W.Y. Lee, M. Wittek, G. Brezesinski, D. Moebius, M. Majda, J. Phys. Chem. B 103 (1999) 6950.
[11] D. Bizzotto, J.J. Noel, J. Lipkowski, J. Electroanal. Chem. 369 (1994) 259.
[12] Y. Yang, D. Bizzotto, J. Electroanal. Chem. 500 (2001) 408.
[13] J.L. Shephard, D. Bizzotto, J. Phys. Chem. B 117 (2003) 8524.
[14] D. Bizzotto, E. Wong, Y. Yang, J. Electroanal. Chem. 480 (2000) 233.
[15] D. Bizzotto, J. Lipkowski Prog. Surf. Sci. 50 (1995) 237.
[16] V. Zamlynny, I. Zawisza, J. Lipkowski, Langmuir 19 (2003) 132.
[17] J.L. Wang, F. Leveiller, D. Jacquemain, K. Kjaer, J. Als-Nelsen, M. Lahav, L. Leiserowitz, J. Am. Chem. Soc. 116 (1994) 1192.
[18] M.C. Shih, T.M. Bohanon, J.M. Mikrut, P. Zschack, P. Dutta, Phys. Rev. A 45 (1992) 5734.
[19] M.K. Durbin, M.C. Shih, A. Malik, P. Zschack, P. Dutta, Coll. Surf. A 102 (1995) 8790.
[20] G. Lautz, Th.M. Fischer, J. Phys. Chem. B 101 (1997) 8790.
[21] G.A. Lawrie, G.T. Barnes, J. Coll. Interf. Sci. 162 (1994) 36.
[22] G. Brezesinski, V.M. Kaganer, H. Mohwald, P.B. Howes, J. Chem. Phys. 109 (1998) 2006.
[23] R. Steitz, J.B. Peng, I.R. Peterson, I.R. Gentle, R.M. Keun, M. Goldmann, G.T. Barnes, Langmuir 14 (1998) 7258.
[24] G. Lautz, Th.M. Fischer, M. Weggand, H. Losche, P.B. Howes, K. Kjaer, J. Chem. Phys. 108 (1998) 4640.
[25] W.D. Harkins, L.E. Copeland, J. Chem. Phys. 10 (1942) 242.
[26] I. Langmuir, V.J. Schaefer, J. Am. Chem. Soc. 60 (1938) 1351.
[27] D. Dickertmann, J.W. Schultze, F.D. Koppitz, Electrochim. Acta 21 (1976) 967.
[28] J. Richer, J. Lipkowski, J. Electrochem. Soc. 133 (1986) 121.
[29] V. Zamlynny, Ph.D. Thesis, University of Guelph, 2002;
(b) M. Hoon-Khoshla, W.R. Fawcett, A. Chen, J. Lipkowski, B. Pettinger, Electrochim. Acta 45 (1999) 611.
[30] M.J. Green, B.J. Barner, R.M. Corn, Rev. Sci. Instrum. 62 (1991) 1426.
[31] B.J. Barner, M.J. Green, E.I. Saez, M.R. Corn, Anal. Chem. 63 (1991) 55.
[32] T. Buffeteau, B. Desbat, D. Blaudez, J.M. Turlet, Appl. Spectrosc. 54 (2000) 1646.
[33] D.L. Allara, J.D. Swalen, J. Phys. Chem. 86 (1982) 2700.
[34] C.R. Flach, A. Gericko, R. Mendelshon, J. Phys. Chem. 101 (1997) 58.
[35] I. Burgess, V. Zamlynny, G. Szymanski, A.L. Schwan, R.J. Faragher, J. Lipkowski, J. Majewski, S. Satija, J. Electroanal. Chem. 550/551 (2003) 187.
[36] C. Braun, The Reflectivity Tool, Parratt 3, HMI, Berlin, 1999.
[37] A. Nelson, A. Benton, J. Electroanal. Chem. 202 (1986) 253.
[38] B.B. Damaskin, O.A. Petrii, V.V. Batrakov, Adsorption of Organic Compounds at Electrodes, Plenum Press, New York, 1971.
[39] D.Y. Kwok, B. Tadros, H. Deol, D. Vollhardt, R. Miller, M.A. Cabrierizo-Vilchez, A.W. Neumann, Langmuir 12 (1996) 1851.
[40] A. Chen, J. Lipkowski, J. Phys. Chem. B 103 (1999) 682.
[41] C.F. Majkrzak, J.F. Ankner, N.F. Berk, D. Gibbs, in: L.H. Bennett, R.E. Watson (Eds.), Magnetic Multilayers, World Scientific Publishing Co., New Jersay, 1994, p. 299.
[42] J. Als-Nielsen, Z. Phys. B 61 (1985) 411.
[43] G. Parratt, Phys. Rev. 95 (1954) 359.
[44] W.N. Hansen, J. Opt. Soc. Am. 58 (1968) 380.
[45] F. Michaud, L. Ventola, M.T. Calvet, M.A. Cuevas-Diarte, X. Solans, M. Font-Bardia, Acta Crystallogr. C 56 (2000) 219.
[46] R.A. MacPhail, H.L. Strauss, R.G. Snyder, C.A. Elliger, J. Phys. Chem. 88 (1984) 334.
[47] R.A. MacPhail, R.G. Snyder, H.L. Strauss, J. Chem. Phys. 77 (1982) 1118.
[48] R.G. Snyder, H.L. Strauss, C.A. Elliger, J. Phys. Chem. 86 (1982) 5145.
[49] P.A. Chollet, J. Messier, C. Rosilo, J. Chem. Phys. 64 (1976) 1048.
[50] K.S. Seshadri, R.N. Jones, Spectrochim. Acta 19 (1963) 1013.
[51] D.L. Allara, A. Baca, C.A. Pryde, Macromolecules 11 (1978) 1215.
[52] J. Umemura, T. Kamata, T. Kawai, T. Takenaka, J. Phys. Chem. 94 (1990) 62.